Vectorial wave-matching mode analysis of integrated optical waveguides

Manfred Lohmeyer
Department of Physics, University of Osnabrück,
Barbarastraße 7, D-49069 Osnabrück, Germany

Abstract: For mode fields of integrated optical waveguides with piecewise constant and rectangular permittivity profile, Maxwell's equations reduce to the twodimensional Helmholtz wave equation, supplemented by continuity requirements on the boundaries between different media. Two basic components of the mode field are expanded into factorizing harmonic or exponential functions, separately on each rectangular region. We determine approximations for guided modes and propagation constants by means of a minimization procedure based on a least squares expression for the mismatch in the continuity requirements. Results for the hybrid mode fields of typical sample waveguides classify this approach as competitive with and superiour to alternative methods for vectorial mode analysis, although some open questions remain.

Keywords: integrated optics, dielectric waveguides, guided modes, numerical modeling

1 Introduction

Frequently dielectric waveguides in integrated optics are fabricated by etching techniques. The waveguide cross sections consist of rectangular pieces, each being filled with a medium of uniform refractive index. While the exact mode analysis of *slab* waveguides with piecewise constant permittivity is fairly easy, for waveguides with twodimensional cross section this task is far more involved. There are no known analytical solutions, an overview over the various numerical techniques can be found in [1, 2].

Recently we proposed an approach ('Wave Matching Method', WMM) [3] which can be understood as an attempt to implement a twodimensional version of the usual procedure for onedimensional slab waveguide analysis. For several standard benchmark problems, the WMM has been shown to be an alternative to other rigorous techniques, like finite differences [4], finite elements [5], the method of lines [6], or the mode matching method [7].

This paper reports on the extension of the former semivectorial to a fully vectorial implementation. In the next section we recall the basic equations for vectorial mode fields and introduce some notation. Section 3 describes the WMM approach and its extension to fully vectorial modes. The last main section shows results for a few sample waveguides. The first two examples are chosen to characterize the behaviour of the vectorial WMM in situations where a semivectorial simulation tool is definitely insufficient, while the last one is a standard benchmark problem.

2 Vectorial mode equations

Consider a partitioning of the waveguide cross section into rectangular regions, each with constant isotropic permittivity, as sketched in Fig. 1. The boundaries are parallel to the transverse x, y coordinate axes, z denotes the direction of propagation.

For a vectorial mode with propagation constant β, the electric field $\boldsymbol{\mathcal{E}}$ and magnetic field $\boldsymbol{\mathcal{H}}$ can be written

$$\boldsymbol{\mathcal{E}}\,(x,y,z,t) = \begin{pmatrix} E_x \\ E_y \\ \mathrm{i}E_z \end{pmatrix}(x,y)\,\mathrm{e}^{\mathrm{i}(\omega t - \beta z)}, \quad \boldsymbol{\mathcal{H}}\,(x,y,z,t) = \begin{pmatrix} H_x \\ H_y \\ \mathrm{i}H_z \end{pmatrix}(x,y)\,\mathrm{e}^{\mathrm{i}(\omega t - \beta z)}, \tag{1}$$

where the components E_x, E_y, E_z and H_x, H_y, H_z of the mode field may be chosen to be real valued quantities. $\omega = kc = 2\pi/\lambda$ is the angular frequency corresponding to the vacuum wavelength λ and speed of light c. The

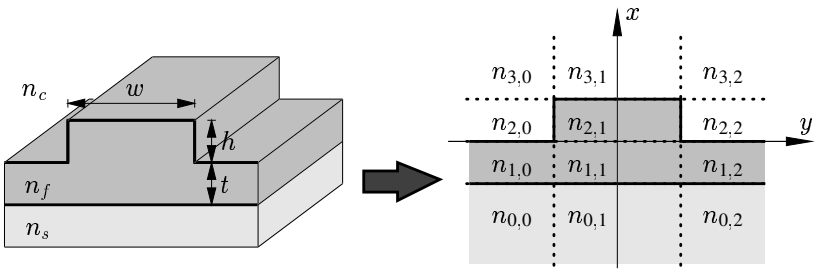

Figure 1: A typical rib waveguide: the cross section plane may be divided into partially unbounded rectangles with uniform refractive index n.

longitudinal components E_z and H_z can be expressed in terms of the transversal components by Maxwell's divergence equations, and electric and magnetic fields are connected by the two curl equations. Therefore it is sufficient to consider only two components for an initial mode calculation. Standard formulations are based on either the transverse electric fields E_x, E_y, the transverse magnetic fields H_x, H_y, or the longitudinal components E_z and H_z.

Since the permittvity is piecewise constant, these two remaining unknown fields Φ_1, Φ_2 satisfy the simple Helmholtz wave equation

$$\partial_x^2\Phi_j + \partial_y^2\Phi_j = (\beta^2 - k^2\epsilon)\Phi_j, \qquad j = 1, 2\,. \tag{2}$$

It applies for almost all points on the cross section plane, except on the boundary lines, where appropriate boundary conditions have to be implemented. On horizontal boundaries (parallel to the y-axis) the quantities ϵE_x, E_y, E_z, H_x, H_y, and H_z are continuous, while on vertical boundaries (parallel to the x-axis) continuity is required for E_x, ϵE_y, E_z, H_x, H_y, and H_z. These conditions must be evaluated in terms of the two basic unknown fields Φ_1, Φ_2 and their first and second order derivatives on the boundary lines.

Note, that the analysis does not start with a set of globally valid differential equations or an equivalent functional. Rather the above formulation emphasizes the viewpoint, that guiding effects as well as polarization coupling arise from the permittivity discontinuity lines only, while inbetween the fields satisfy the equation for electromagnetic waves in an infinite homogeneous medium.

Frequently a waveguide is mirror symmetric with respect to the transformation $y \to -y$, and the modes have a definite parity. For a single mode, Maxwell's equations demand equal parity for H_x, E_y, and H_z, and reversed parity for E_x, H_y, and E_z. Throughout this paper, we call a hybrid mode with even H_x, E_y, and H_z symmetric, one with these components odd will be denoted antisymmetric.

3 Wave matching method

On each rectangular region, the two basic fields Φ_1, Φ_2 are assumed to be sums

$$\Phi_j(x, y) = \sum_l a_{jl}\phi_{jl}(x, y) \tag{3}$$

of factorizing real solutions ϕ_{jl} of the wave equation (2) with real coefficients a_{jl}. These trial functions ϕ_{jl} are of the form

$$\phi(x, y) = c \cdot F(p(x - x_0)) \cdot G(q(y - y_0))\,, \tag{4}$$

where F and G are one of the functions sin, cos, or exp. c is a normalization constant and x_0, y_0 are introduced as local coordinate offsets. Then the transverse wave vector components p, q satisfy an equation

$$\pm\, p^2 \pm q^2 = \beta^2 - k^2\epsilon\,. \tag{5}$$

To restrict the number of trial functions, suitable subsets of parameters p, q must be selected from the sets prescribed by Eq. (5), separately on each rectangle and for each choice for F and G. This should be done in such a way that the space spanned by the selected trial functions is sufficiently large, while at the same time these functions are numerically linearly independent. In [3] we have described a quite universal procedure for such a spectral discretization in detail.

On the outer, unbounded rectangles only outwards exponentially decaying trial functions are considered. The WMM needs no spatial computational window, the mode functions are defined on the entire waveguide cross section plane.

Once the systems of trial functions are fixed, the continuity requirements must be incorporated to connect neighbouring regions. This is done by integrating the squared differences in the electric and magnetic fields along the horizontal boundary lines C_h and vertical lines C_v. The resulting expression is to be considered a function of all coefficients $\boldsymbol{a}$ and of the searched for propagation constant β:

$$\begin{aligned} D_\beta(\boldsymbol{a}) &= \sqrt{\epsilon_0}\int_{C_h}\left\{((\epsilon E_x)^+-(\epsilon E_x)^-)^2+(E_y^+-E_y^-)^2+(E_z^+-E_z^-)^2\right\}\,\mathrm{d}y \\ &+ \sqrt{\mu_0}\int_{C_h}\left\{(H_x^+-H_x^-)^2+(H_y^+-H_y^-)^2+(H_z^+-H_z^-)^2\right\}\,\mathrm{d}y \\ &+ \sqrt{\epsilon_0}\int_{C_v}\left\{(E_x^+-E_x^-)^2+((\epsilon E_y)^+-(\epsilon E_y)^-)^2+(E_z^+-E_z^-)^2\right\}\,\mathrm{d}x \\ &+ \sqrt{\mu_0}\int_{C_v}\left\{(H_x^+-H_x^-)^2+(H_y^+-H_y^-)^2+(H_z^+-H_z^-)^2\right\}\,\mathrm{d}x\,. \end{aligned} \tag{6}$$

Superscripts $+$ and $-$ indicate fields (3) assigned to neighbouring rectangles on opposite sides of the boundary, where the functions are evaluated exactly on the boundary line. The roots of the vaccuum permittivity ϵ_0 and permeability μ_0 have been introduced to adjust the dimensions of the electric and magnetic components. If these are expressed in terms of two basic fields Φ_1, Φ_2 and scaled for numerical purposes, the weighting factors $\sqrt{\mu_0}$, $\sqrt{\epsilon_0}$ ensure a balanced influence of the discontinuities in E and H on the overall field mismatch.

Although the least squares expression has been chosen somewhat arbitrarily, (cf. the corresponding remarks in [3]), vanishing of $D_\beta(\boldsymbol{a})$ for a parameter β and nonzero $\boldsymbol{a}$ characterizes a mode field exactly. Nevertheless, since we deal with a partial differential equation of second order in both transverse directions, one would expect that four boundary conditions (one for the field and one for the normal derivative of the two basic components) are sufficient. By inspection of Maxwell's equation it can be shown that exact continuity of H_x, H_y, H_z and E_z implies the appropriate behaviour for E_x and E_y, provided that Eq. (2) holds for all components. Indeed we have found indications that an expression for D like Eq. (6) with the E_x and E_y terms dropped may provide better convergence (see Sec. 4.3). However, in other situations, e.g. for the structure in Sec. 4.2, this modification leads to less reasonable fields where the mismatch is concentrated in the dropped components. Therefore we stick to the original expression (6).

Only normalized fields may be compared with respect to the field mismatch. For this purpose we adopted one of the common expressions

$$N_\beta(\boldsymbol{a}) = \iint\left\{E_x^2+E_y^2+E_z^2\right\}\,\mathrm{d}x\,\mathrm{d}y \tag{7}$$

and

$$N_\beta(\boldsymbol{a}) = \iint\left\{H_x^2+H_y^2+H_z^2\right\}\,\mathrm{d}x\,\mathrm{d}y\,. \tag{8}$$

With the restricted set of trial functions an exact representation of the mode field will not be feasible. One can expect, that the minimum achievable mismatch will be small if β is close to a valid propagation constant. This assumption forms the basis of the procedure to determine the propagation constants: In a first step, for a given trial value β, an optimum normalized coefficient vector $\boldsymbol{a}$ with corresponding minimum remaining mismatch $\mu_\beta = D_\beta(\boldsymbol{a})$ is calculated. In a second step the mismatch μ_β is minimized with respect to β. The locations of the minima yield approximations to the propagation constants.

The implementation of this procedure starts with analytic evaluating all integrals in the expressions for D and N. Both reduce to simple quadratic forms,

$$D_\beta(\boldsymbol{a}) = \boldsymbol{a}\mathsf{D}_\beta\boldsymbol{a}\,, \qquad N_\beta(\boldsymbol{a}) = \boldsymbol{a}\mathsf{N}_\beta\boldsymbol{a}\,, \tag{9}$$

where D_β and N_β are real positive matrices. Consequently, μ_β can be calculated from the eigenvalue equation

$$\mathsf{D}_\beta\boldsymbol{a} = \mu_\beta\mathsf{N}_\beta\boldsymbol{a}\,. \tag{10}$$

This numerical procedure is identical to the semivectorial case and has been reported in detail in Ref. [3].

A consistent theoretical assessment for this method is still lacking. Such an assessment should comprise a variational principle as a basis for the numerical error minimization procedure. In particular, it should identify expressions for the least squares error (6) and the normalization (7,8) that yield in some way best estimates of the propagation constants for a trial field. However, from our experience we conclude that, if not the best, (6-8) are at least good choices.

4 Results

In each calculation the spectral discretization process, i.e. the selection of wave vector components p, q according to Eq. (5), is governed by three parameters: a lower limit d for the difference between trial functions with neighbouring p, q, second a parameter $\alpha_{\max}$ for the maximum value p or q, resp. , and third the maximum number of elements N_α in each set of trial functions. For completeness, these parameters are presented in this paper, too; cf. Ref. [3] for their precise meaning.

Note that all numerical results given in this and the previous paper have been calculated with the same spectral discretization parameters (but with quite different total numbers of trial functions, since their number depends on e.g. refractive index values, number and dimension of rectangles, or the propagation constant). The modal indices given are stable with respect to a refinement of the spectral discretization, thus the choice of suitable discretization parameters does not depend crucially on the structure under consideration.

Smaller trial function sets were used for initially scanning the interval of possible propagation constants. On this occasion we have found that a certain small minimum density of the spectral discretization is necessary for minima related to specific modes to appear in the least squares error function. However, it was never a problem to exceed this minimum density.

For a basic rectangular waveguide, e.g. the square core of Sec. 4.2, a complete run of the vectorial WMM program with accuracy as given takes about 7 min on a 99 MHz HP 735 computer, output of all data for Fig. 4-6 included. About 5 MB of memory are needed. The method is therefore well qualified for an implementation on usually faster personal computers. Note that both time and memory consumption scale with the number of unknowns in the eigenvalue problem (10), i.e. with the number of rectangles and the density of the spectral discretization, where the simple iterative eigenvalue solver of the current implementation leaves much room for optimization. In terms of computational effort, the method should be competitive with the modal transverse resonance method [7], while the memory requirements of vectorial FE or FD methods are an order of magnitude larger.

4.1 Raised strip waveguide

The first example is intended to provide a consistency check for the implemented algorithms. The structure consists of a single rib of increased refractive index on a substrate surface. It is simulated twice, first with the substrate surface parallel to the y-axis of the simulation tool, second with this plane parallel to the x-axis.

As expected, the fields from calculations in the two configurations are connected exactly by the rotation $H_x \to H_y$, $H_y \to -H_x$. Note, that this result was obtained by exchanging the values for the refractive indices and the layer surfaces only. No parameters had to be adjusted, which assume a different field behaviour in the transverse directions.

Tab. 1 exhibits the propagation constants of the four guided modes which the WMM has found. As usual, the strictly speaking hybrid modes are classified by the dominant field components. The index indicates the number of lines on the cross section plane where the field vanishes. For fixed spectral discretization, the precision of the propagation constants remains stable with respect to the formulation of the vectorial mode problem (i.e. use of one of the pairs (H_x, H_y), (E_x, E_y), or (E_z, H_z) as basic fields) and with respect to the choice of the normalization function (Eq. (7) or (8)).

	TE_0	TM_0	TE_1	TM_1
$\beta/\mu\text{m}^{-1}$	10.3432	10.1192	9.9994	9.8162
N_{tf}	640	644	653	657

Table 1: Propagation constants β and the total number N_{tf} of trial functions used in the WMM calculation for the modes of a strip waveguide with the following parameters (cf. Fig. 1): refractive indices $n_s = 1.95$, $n_f = 2.302$, $n_c = 1.0$, rib width and height $w = 2.0\,\mu$m, $h = 0.54\,\mu$m, vacuum wavelength $\lambda = 1.3\,\mu$m.

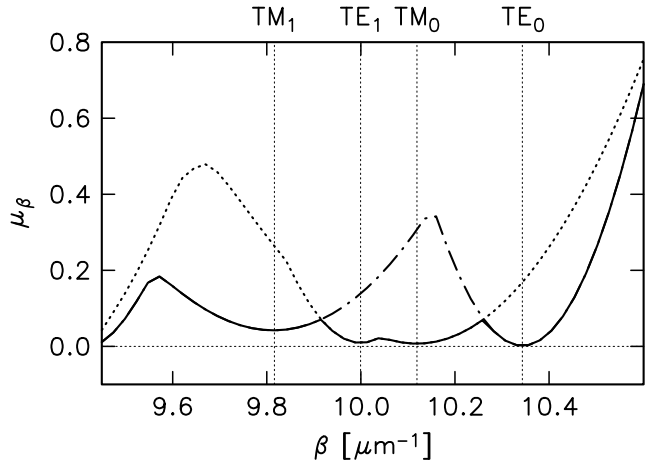

Figure 2: Minimum field mismatch $\mu_\beta = D_\beta(\boldsymbol{a})$ for normalized fields versus the trial parameter β. The continuous line corresponds to fields without prescribed symmetry, the dash-dotted and dotted lines (partially shadowed) to fields with even and odd symmetry. See the caption of Tab. 1 for parameters.

For each mode, the number of unknowns N_{tf} in Tab. 1 corresponds to a field ansatz of proper symmetry. The same results can be obtained without prescribing the symmetry, as illustrated in Fig. 2. It shows the remaining field mismatch $D_\beta(\boldsymbol{a})$ for optimum coefficient vectors $\boldsymbol{a}$. The μ_β curves consist of parabolic sections, where each section is associated with a valid propagation constant at the minimum. From the calculation without prescribed symmetry we got a superposition of the curves for even and odd symmetry, where for each β the smaller eigenvalue μ_β has been selected.

Note that the locations of the minima in the μ_β curves depend on the spectral discretization density. Convergence as mentioned above is to be understood in the sense of stability of these locations versus spectral discretization refinement. Although the minima in Fig. 2 might appear rather shallow, evaluation of the relevant abscissas with sufficient precision poses no problem.

4.2 Buried square waveguide

From [8] we adopted the second sample structure, a square guiding core surrounded by air as sketched in Fig. 3.

The spectral discretization $d = 0.01$, $\alpha_{\max} = 3.0$, $N_\alpha = 30$ leads to a mode function which is a superposition of 554 trial functions. Fig. 4 surveys the corresponding field profiles. We have selected one of the two orthogonal fundamental modes with a field ansatz of proper symmetry. An ansatz with reversed symmetry yields the same propagation constant $\beta = 5.3212\,\mu\text{m}^{-1}$ and identical field profiles, apart from changes due to the transformation $x \to y$, $y \to -x$.

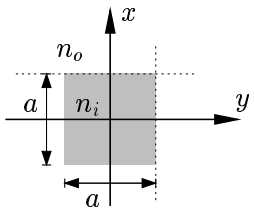

Figure 3: Square waveguide cross section. Parameters of the simulated structure are height and width of the core $a = 1.0\,\mu$m, wavelength $\lambda = 1.5\,\mu$m, and core and cladding refractive indices $n_i = 1.5$, $n_o = 1.0$.

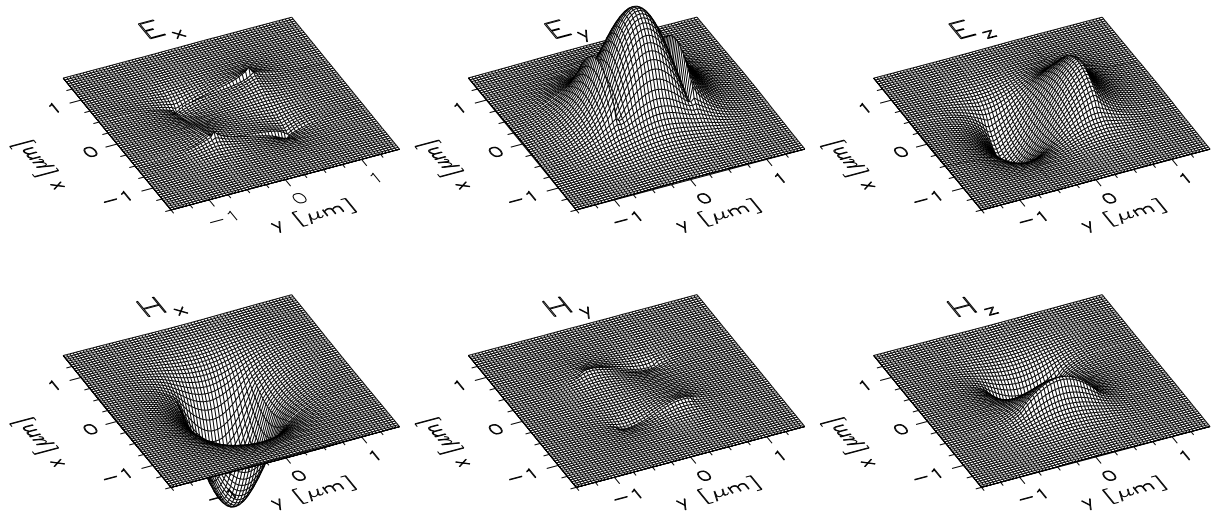

Figure 4: Amplitudes of the electric (top row) and magnetic field components (bottom row) plotted versus the cross section plane, for the square waveguide of Fig. 3. Values are comparable within each row.

For a more quantitative illustration of the mode shape we have evaluated the mode field on a series of horizontal and vertical lines in the x-y-plane, as displayed in Fig. 5 and 6. The maximum amplitudes of the dominant transverse electric and magnetic components E_y, H_x can be read from Fig. 5. These maximum levels should be kept in mind when examining the fields at the edges of the core. Note, that the minor fields E_x, H_y are zero along both transverse coordinate axes due to the prescribed symmetry.

Fig. 6 allows for a detailed inspection of the remaining mismatch on the boundaries of the basic rectangular sections. On the lines $x = a/2$ and $y = a/2$ we have plotted two curves for each field component, one where the fields on the core rectangle are evaluated (continuous curves), and one for the field on the neighboured rectangle outside the core (dotted curves). Apart from the normal components of the dielectric displacement the continuous and dotted curves should coincide, while for E_x on the horizontal section $x = a/2, -a/2 < y < a/2$ and for E_y on the vertical section $y = a/2$, $-a/2 < x < a/2$ the dotted curve should be 2.25 times the level of the continuous curve. Obviously at the waveguide corners these conditions are contradictory for finite field amplitudes, and the electromagnetic fields are known to be divergent there [9]. Nevertheless, at least qualitatively, the main features of the divergent behaviour can be approximated with a finite number of exponentials. The reader may compare the upper right quadrant of Fig. 6, top left inset, with a corresponding plot in [8] (note the additional boundary conditions).

4.3 Rib waveguide

The structure employed as the last example has frequently been the subject of computations when comparing different mode solvers. It comprises a deeply etched rib with geometry parameters $w = 2.0\,\mu$m, $h = 1.1\,\mu$m, and $t = 0.2\,\mu$m (cf. Fig. 1), refractive indices, $n_s = 3.34$, $n_f = 3.44$, and $n_c = 1.0$ for a wavelength of $\lambda = 1.55\,\mu$m. Tab. 2 summarizes effective mode indices for the fundamental mode from a few reference methods and the semivectorial and vectorial WMM. Further results for this waveguide are collected in [4, 10, 11, 3].

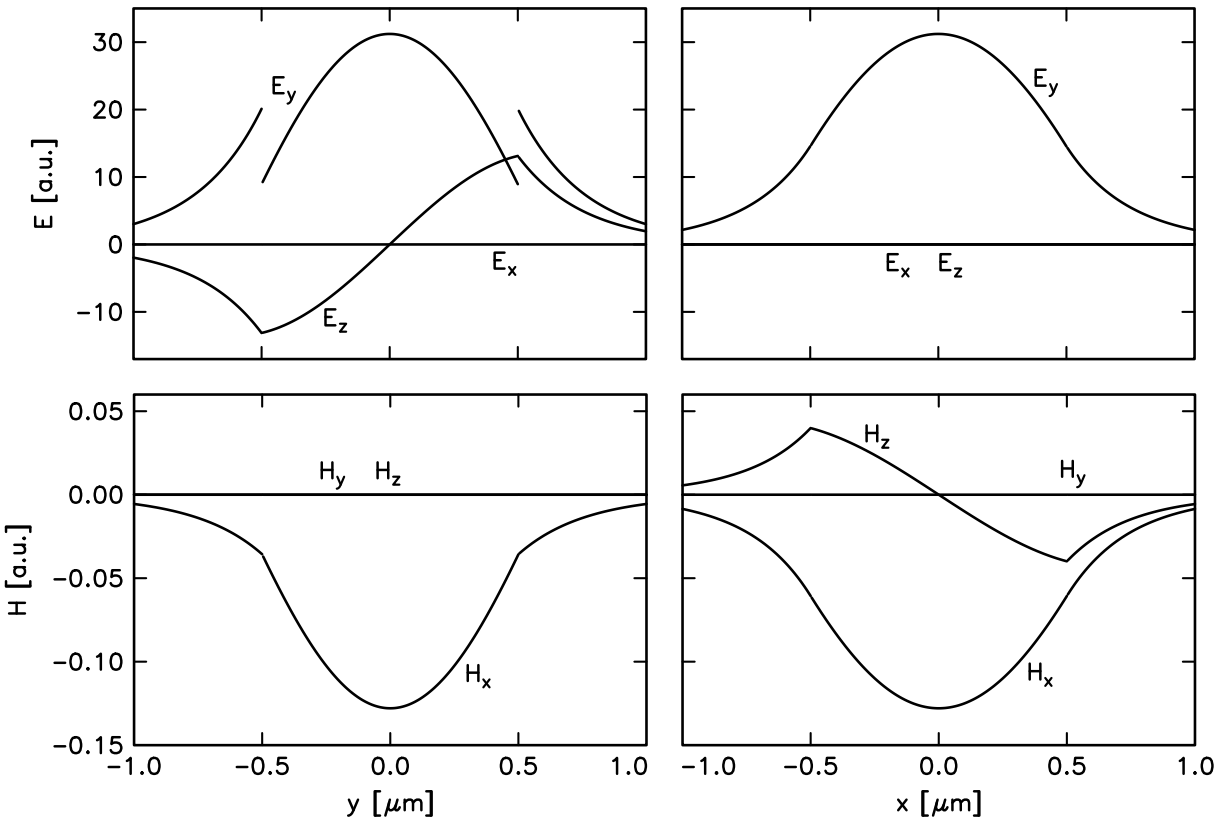

Figure 5: For the square waveguide of Fig. 3: electric (top row) and magnetic (bottom row) field amplitudes evaluated on the y-axis (left column) and on the x-axis (right column).

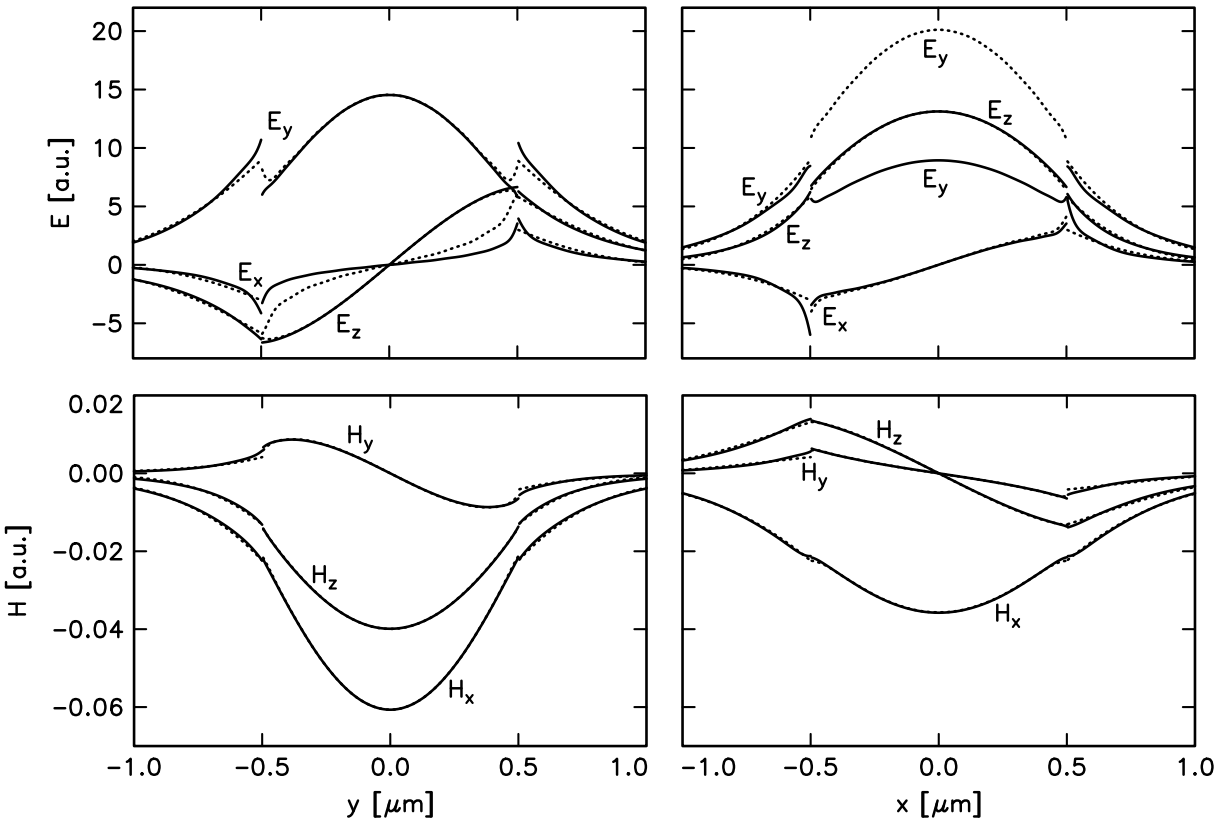

Figure 6: For the square waveguide of Fig. 3: electric (top row) and magnetic (bottom row) field amplitudes evaluated on the horizontal line at the top edge of the core (left column) and the vertical line at the right edge (right column). Continuous curves correspond to locations $(x, y) = (a/2 - \delta, y)$ or $(x, a/2 - \delta)$, resp., while dotted curves are assigned to coordinates $(a/2 + \delta, y)$ and $(x, a/2 + \delta)$, for a small deviation δ.

	β/k	B
SFDM	3.388646	0.48278
TRD	3.388690	0.48325
SWMM	3.388659	0.48291
$VFDM_1$	3.388687	0.48319
$VFDM_2$	3.388698	0.48330
MTRM	3.388698	0.48330
VWMM*	3.388669	0.48301
VWMM	3.388573	0.48214

Table 2: Effective mode indices β/k and normalized propagation constants $B = ((\beta/k)^2 - n_s^2)/(n_f^2 - n_s^2)$ for the benchmark waveguide. VFDM: vectorial finite difference calculations by P. Lüsse et al. [4] ($VFDM_1$) and [10] ($VFDM_2$); MTRM: vectorial mode transverse resonance method by A. Sudbø[7], data from [10]; TRD: semivectorial transverse resonance diffraction method by T. Rozzi et al. [12]; SFDM: semivectorial finite difference implementation by P. Lüsse et al. [13]; SWMM: our previous semivectorial wave matching program [3]; VWMM: the present vectorial implementation, VWMM*: calculation without the E_x and E_y terms in the mismatch expression Eq. (6).

The first three rows of Tab. 2 contain results of semivectorial calculations. They agree up to the third digit in the normalized propagation constant, and there is very good agreement with the vectorial values from the subsequent rows. Thus the semivectorial approximation, i.e. putting E_x zero, is a good approximation for this waveguide. This can also be concluded from the plots in Fig. 7, where the amplitudes of the small components E_x and H_y clearly appear to be negligible. The displayed fields correspond to the last row in Tab. 2. They are composed from a trial function set with 879 unknown coefficients, the spectral discretization parameters are $d = 0.01$, $\alpha_{\max} = 3.0$, and $N_\alpha = 30$.

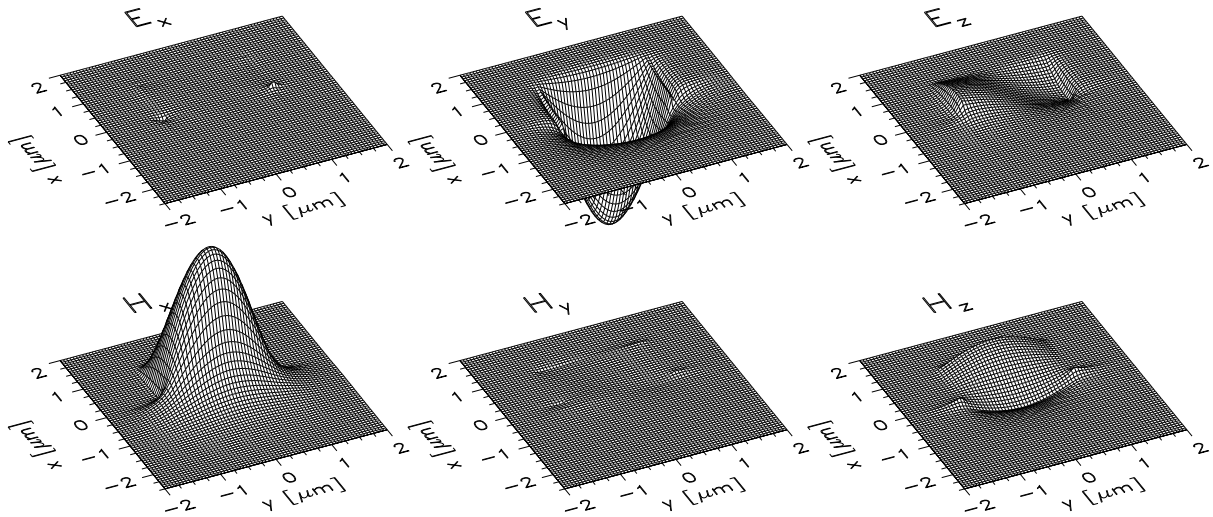

Figure 7: Amplitudes of the electric (top row) and magnetic field components (bottom row) plotted versus the cross section plane, for the waveguide considered for Tab. 2. Values are comparable within each row.

Unfortunately there is a noticeable discrepancy between the WMM effective mode index from the last row of Tab. 2 and the previous values. This difference vanishes for the semivectorial WMM program. Therefore a reason may be found in the more irregular shape of the small components, e.g. the divergent peaks at the waveguide edges, where the spectral discretization employed here is less sufficient.

As can be seen from the row marked VWMM*, the deviation is significantly reduced, if one modifies the expression for the least squares error in the continuity requirements (cf. Sec. 3), such that only continuity of H_x, H_y, H_z, and E_z is explicitely incorporated. Fig. 8 compares the transverse magnetic components of the corresponding fields. While the dominant component H_x is not visibly influenced, the shape of the minor one H_y changes significantly.

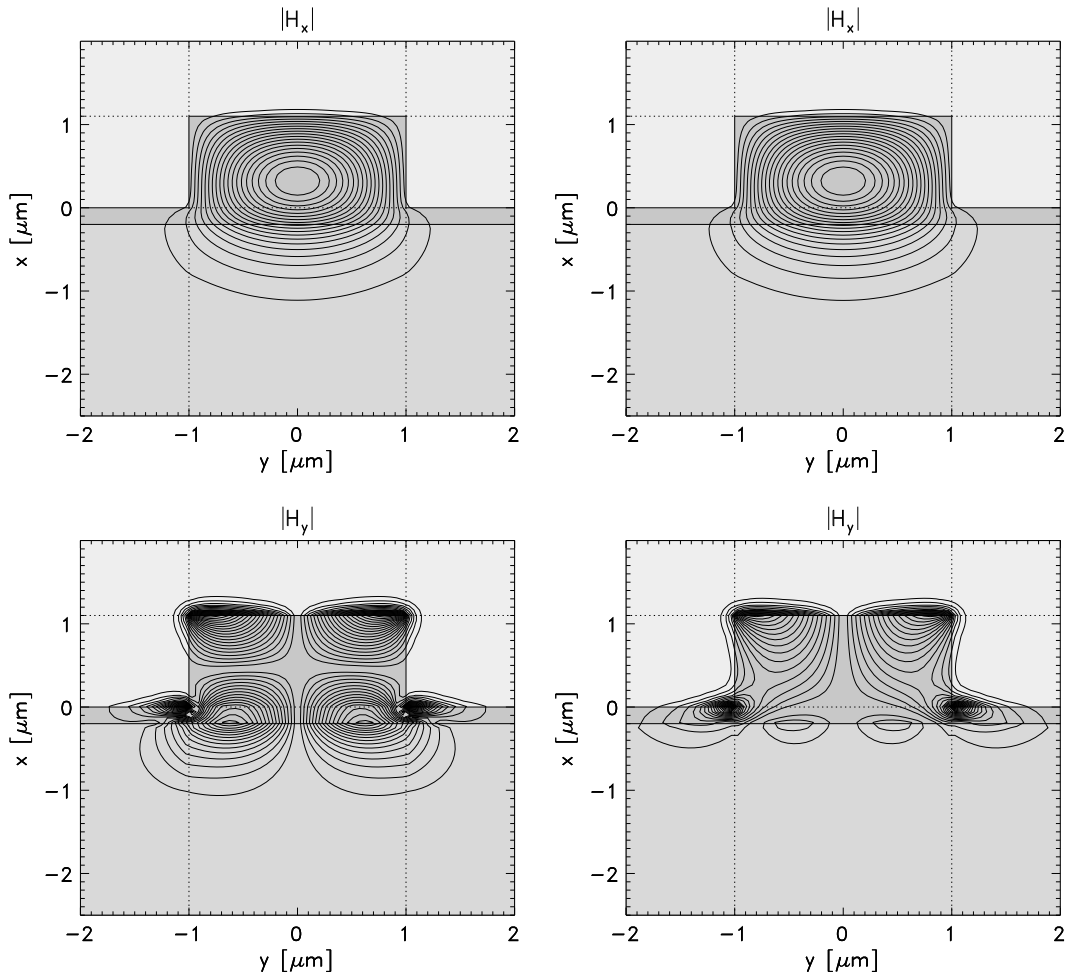

Figure 8: Transverse magnetic fields for the waveguide of Tab. 2, from vectorial WMM calculations with error expression (6) (left column) and without the E_x and E_y Terms in (6) (right column). The contour levels are spaced by 5% of the maximum absolute field, separately for each plot. Note that the clippings from the waveguide cross section are chosen for displaying purposes only, there is no spatial computational window. Horizontal and vertical lines indicate the refractive index profile and its splitting into rectangular sections.

Similar plots in [10] agree well with the right column of Fig. 8. In addition to good agreement of the values for the normalized propagation constants, this recommends the reduced least squares expression as the better choice if one accepts the results taken from [10] as correct. However, there are two reasons to be suspicious about this finding. The finite difference scheme (on which the VFDM_2 value is based) employs the continuity requirements for the three magnetic components and the longitudinal electric component as well. This is correct if the continuity requirements are fulfilled exactly, but probably not in the sense of a balanced approximation of all six fields. Further, for structures with less negligible minor components (e.g. the waveguide of Sec. 4.2), fields computed with the reduced least squares expression show a more irregular appearance, where the error is concentrated in the continuity requirements for the dropped components E_x, E_y.

5 Conclusions

We have shown that the semivectorial WMM can be successfully extended to fully vectorial simulations. The positive features remain: There is no spatial computational window; with moderate computational resources the method yields accurate quasianalytic approximations for all electromagnetic field components. These fields form an ideal basis for further processing within a larger tool for integrated optics design, e.g. in the framework of perturbation theory or as initial fields for beam propagation.

The vectorial WMM performs truly vectorial calculations in the sense that both transverse directions are treated

alike. While the piecewise defined trial fields are well suited to deal with field discontinuities or discontinuous derivatives, divergent peaks in the corners of dielectric waveguides are less sufficiently approximated (as is the case for most other schemes). The method yields the qualitative features of the field behaviour in these regions only. However, if not necessarily factorizing but numerically applicable divergent solutions of the wave equation in such a corner would be available, it should be possible to incorporate them. Approximate analytical solutions may be sufficient, e.g. the fields given in [9].

One drawback remains: it is not obvious what happens for closely spaced propagation constants where the parabolic pieces in the WMM error function (see Fig. 2) are superimposed for two different hybrid modes. Frequently, for waveguides with mirror symmetry, this can be overcome by enforcing an appropriate symmetry of the solution. However, there are certain configurations where modes with the same symmetry have nearly equal propagation constants. There are even applications relying on such structures [14]. Maybe an ansatz to deal with this situation is to exploit the freedom in the choice of the normalization expression to identify the different parabolic sections of the error function which correspond to the degenerate modes.

Acknowledgment

The author would like to thank N. Bahlmann and P. Hertel for valuable discussions and for critically reading the manuscript.

References

[1] K. S. Chiang. Review of numerical and approximate methods for the modal analysis of general optical dielectric waveguides. *Optical and Quantum Electronics*, 26:S113–S134, 1994.

[2] C. Vassallo. 1993-1995 Optical mode solvers. *Optical and Quantum Electronics*, 29:95–114, 1997.

[3] M. Lohmeyer. Wave-matching method for mode analysis of dielectric waveguides. *Optical and Quantum Electronics*, 29:907–922, 1997.

[4] P. Lüsse, P. Stuwe, J. Schüle, and H.-G. Unger. Analysis of Vectorial Mode Fields in Optical Waveguides by a New Finite Difference Method. *Journal of Lightwave Technology*, 12(3):487–493, 1994.

[5] B. M. A. Rahman and J. B. Davies. Vector-H Finite-Element Solution of GaAs/GaAsAs Rib Waveguides. *IEE Proceedings*, 132(6):349–353, 1985.

[6] U. Rogge and R. Pregla. Vectorial Method of Lines for the Analysis of Strip-Loaded Optical Waveguides. *Journal of the Optical Society of America B*, 8:459–463, 1991.

[7] A. S. Sudbø. Film mode matching: a versatile numerical method for vector mode fields calculations in dielectric waveguides. *Pure and Applied Optics*, 2:211–233, 1993.

[8] A. S. Sudbø. Why Are Accurate Computations of Mode Fields in Rectangular Dielectric Waveguides Difficult ? *Journal of Lightwave Technology*, 10(4):418–419, 1992.

[9] M. Bressan and P. Gamba. Analytical Expressions of Field Singularities at the Edge of Four Right Wedges. *IEEE Microwave and Guided Wave Letters*, 4(1):3–5, 1994.

[10] P. Lüsse. *Numerische Entwurfswerkzeuge für optische Wellenleiterbauelemente*. VDI - Verlag, Düsseldorf, 1997. VDI Fortschritts-Berichte, Reihe 20: Rechnerunterstützte Verfahren, Nr. 239.

[11] H. Noro and T. Nakayama. A New Approach to Scalar and Semivector Mode Analysis of Optical Waveguides. *Journal of Lightwave Technology*, 14(6):1546–1556, 1996.

[12] T. Rozzi, G. Cerri, M. N. Husain, and L. Zappelli. Variational Analysis of the Dielectric Rib Waveguide Using the Concept of "Transition Function" and Including Edge Singularities. *IEEE Transactions on Microwave Theory and Techniques*, 39(2):247–257, 1991.

[13] P. Lüsse, K. Ramm, and H.-G. Unger. Comparison of a vectorial and new semivectorial finite-difference approach for optical waveguides. *Optical and Quantum Electronics*, 29:115–120, 1997.

[14] K. Mertens, B. Scholl, and H. J. Schmitt. New Highly Efficient Polarization Converters Based on Hybrid Supermodes. *Journal of Lightwave Technology*, 13(10):2087–2092, 1995.